BREAKTHROUGH REPORT

Quantitative cell release from plant tissues for single-cell genomics

D. Blaine Marchant[a,†], Brad Nelms[a,b,†], Virginia Walbot[a]

Corresponding authors. Email: danielm1@stanford.edu (DBM); nelms@uga.edu (BN); walbot@stanford.edu (VW)

[a]Department of Biology, Stanford University, Stanford, CA 94305, USA

Footnotes

[b]Current address: Department of Plant Biology, University of Georgia, Athens, GA 30602

[†]DBM and BN contributed equally to this work

Short title: Fixation-based scRNA-seq

The author responsible for distribution of materials integral to the findings presented in this article in accordance with the policy described in the Instructions for Authors (www.plantcell.org) is D. Blaine Marchant (danielm1@stanford.edu).

ABSTRACT

Single-cell RNA-sequencing (scRNA-seq) can provide invaluable insight into cell development, cell type identification, and plant evolution. However, the resilience of the cell wall makes it difficult to dissociate plant tissues and release individual cells. Here, we show that plant tissues can be rapidly and quantitatively dissociated if the tissues are fixed prior to enzymatic digestion. Fixation enables digestion at high temperatures at which enzymatic activity is optimal and stabilizes the plant cell cytoplasm, rendering cells resistant to mechanical shear force. This protocol was applied to maize anthers and provided suitable single-cell expression data for the identification of the tapetum, endothecium, meiocytes, and epidermis, while providing putative marker genes and gene ontology information for the identification of unknown cell types. This approach also preserves morphology of the isolated cells, permitting many cell types to be identified without staining. Our fixation-based protocol can be applied to a range of plant species and tissues with minimal optimization.

INTRODUCTION

The cell holds the genetic blueprint of an organism, yet neighboring cells can differ dramatically in morphology and function. Understanding the gene expression patterns that lead to these differences can provide profound insight into the role, developmental trajectory, and evolution of cell types, tissues, and even organisms. Single-cell RNA sequencing (scRNA-seq) has catalyzed our understanding of animal cells leading to major breakthroughs in cell biology (Han et al., 2020), medicine (Lim et al., 2020; Paik et al., 2020), and evolution (Kanton et al., 2019); however, the usage of scRNA-seq in plants has been hampered largely by the presence of the cell wall, which complicates the separation and isolation of single cells (Seyfferth et al., 2021).

Plant biologists have largely overcome this hurdle by enzymatically digesting, or protoplasting, the wall of living plant cells (Nelms and Walbot, 2019; Zhang et al., 2019; Liu et al., 2021; Lopez-Anido et al., 2021; Denyer et al., 2019). This step has been rate-limiting in implementing scRNA-seq as the needed enzymes, enzyme concentrations, digestion time, and digestion conditions vary depending on the species and tissue under investigation. Inadequate protoplasting can result in cell type biases, cell clumps, cell debris, mRNA leakage, or cell lysis, all of which will interfere with the downstream processing needed for scRNA-seq. Even with an

optimized protocol, the protoplasts can have ectopic expression patterns as a result of the digestion treatment (Denyer et al., 2019) and are extremely fragile.

In response to these limitations, one solution has been to use single nucleus RNA-sequencing (snRNA-seq) in which the plant cells are lysed to release the intact nuclei (Conde et al., 2021; Sunaga-Franze et al., 2021). The nuclei are then isolated and the total nuclear RNA can be reverse transcribed and sequenced. Although snRNA-seq has the benefit of avoiding cell protoplast preparation, nuclear RNA is sequenced but not cytoplasmic mRNA. As a result, there is significantly less RNA per cell, less sensitive detection of rare transcripts, an inability to detect distinct isoforms, and a more transient analysis of expression compared to scRNA-seq as transcripts are known to accumulate in the cytoplasm and vary in abundance there over time among different cell types (Sunaga-Franze et al., 2021; Thrupp et al., 2020).

To date, the majority of plant scRNA-seq studies have focused on the root tip of *Arabidopsis thaliana* as it has relatively few cell types, established protoplast protocols, and numerous cell type marker genes (Denyer et al., 2019; Jean-Baptiste et al., 2019; Ryu et al., 2019; Zhang et al., 2019). Even in such a well-studied system, these analyses have been instrumental in establishing and refining the spatial and temporal development of the different cell types (Denyer et al., 2019; Zhang et al., 2019), identifying new marker genes for rare cell types (Denyer et al., 2019), and discovering the genetic basis for mutant phenotypes (Ryu et al., 2019). Expanding both the taxonomic and tissue breadth of scRNA-seq research in plants can address questions related to all realms of basic and applied plant sciences.

Here, we show that plant cells can be released more efficiently if plant tissues are fixed prior to enzymatic digestion (Figure 1). Fixation provides two key benefits for cell release: it (i) stabilizes the cell cytoplasm so that cells can withstand harsher shear forces without breaking, and (ii) allows enzymatic digestion to occur at higher temperatures (~50°C) where the cellulase enzymes are most active (Pardo and Forchiassin, 1999). RNA is maintained by fixation and can be extracted for later analysis by scRNA-seq. We quantified the cell release of the fixation-based protocol to that of established protoplasting protocols in maize anthers and root tips and demonstrated the ability to perform scRNA-seq of cells released from fixed plant tissue using maize anthers as our model system. We also found that our protocol could readily be applied to non-model plant systems and that fixation maintains cellular morphology after cell wall digestion. This is a critical divergence from previous protoplast-based cell isolation methods as

cell morphology is often the sole means of differentiating cell types in taxa lacking cell type marker genes. Maize anthers provide an ideal test system for scRNA-seq as the cell type composition of the anther, morphology, and development of the anther cell types are well-documented (Figure 1, B-D)(Kelliher and Walbot, 2011), yet varying degrees of background knowledge (marker genes, biological function, developmental trajectory) exist regarding the genetic activity for each cell layer. This protocol can be broadly applied to a variety of taxa and tissues with little optimization to provide high-quality scRNA-seq data, thus permitting scalable single-cell research throughout the many study systems of plant biology.

RESULTS

Fixation increases cellular release of plant tissues

Cell isolation is perhaps the largest hurdle in single-cell RNA-seq of plant tissues. To determine the possible benefits of fixation on cell isolation, we quantified cellular release of fixed plant cells and fresh protoplasts in both maize anthers and maize root tips. We found that a standard optimized maize anther protoplast protocol (Nelms and Walbot, 2019) had a mean release of 4,387 cells per anther when digested for 90 min and 11,333 cells per anther when extended to 16 h (Figure 2A). In comparison, if anthers were fixed prior to digestion, 15,900 cells were released within 90 minutes; this increase in cell release is presumably because the cells were stabilized against mechanical lysis by fixation, while unfixed protoplasts are very fragile. When incubation temperature was increased from 30°C (standard) to 50°C we observed an average release of 45,033 isolated cells (Figure 2), close to the theoretical number of cells in a 2.0 mm maize anther (Kelliher and Walbot, 2011). The standard protoplasting protocol released very few epidermal and endothecial cells, which tended to remain clumped and undigested, producing a skewed release of tapetal cells, middle layer cells, and meiocytes. When the anthers were fixed then digested at 50°C we did not observe any cell clumps, debris, or undigested material, suggesting that the digestion was complete (Supplemental Figure 1). In addition to increasing the cell release efficiency and cell type uniformity, we found that fixation prior to digestion maintained cells' natural morphology allowing the potential for cell type identification post-isolation (Supplemental Figure 1B).

To test the applicability of this protocol to other tissues, we quantified cell release from maize primary root tips after dissociation using: (i) an established maize root tip protoplasting

protocol (Ortiz-Ramírez et al., 2018); (ii) our fixed-cell method with the enzyme mix from Ortiz-Ramírez et al. (2018); (iii) our fixed-cell method with a reduced enzyme mix. Root tips digested by live tissue protoplasting released 24,667 cells per root tip, similar to what has been reported in the literature (Ortiz-Ramírez et al., 2018). In contrast, root tips that were fixed then digested at higher temperatures released approximately four times as many cells (Figure 2B). Similar to the results we found in anthers, fixed root tips showed little evidence of cell clumps or debris after digestion, suggesting that nearly all cells were released from the tissue. Protoplasting protocols can be difficult to establish for new tissues. For instance, Ortiz-Ramirez et al. (2018) used a complex protocol to achieve adequate cell release from root tips, including a four-enzyme blend and pretreating live root tissue with L-cysteine. After fixation, we obtained equivalent cell release from roots when using the four-enzyme blend and L-cysteine pretreatment of Ortiz-Ramirez et al. (2018) or using our simpler two-enzyme blend without any treatments (Figure 2B), suggesting the approach might be applied to new tissues with minimal optimization. To test this premise, we applied our fixed-cell protocol to two non-model systems, leaf tissues from *Amborella trichopoda* and waterlily (*Nymphaea colorata*). We found that the cells of both species readily dissociated and maintained their morphology with no additional optimization of the protocol (Supplemental Figures 1, C and D).

Enzyme purification is necessary for maintaining RNA quality

While fixation itself does not affect RNA quality, it removes the cell membrane and makes the internal RNA contents accessible to RNases in solution. This creates a challenge during enzymatic digestion because most cell wall digesting enzymes are complex mixtures that contain substantial RNase activity. We tested a range of RNase inhibitors, including commercial inhibitors, EDTA, and vanadyl ribonucleoside complexes, but found none that could effectively inhibit the RNase activity in cellulase enzyme blends. This is partly because many available RNase inhibitors target the RNase A family of RNases (MacIntosh, 2011), which is only produced in vertebrates. Secreted fungal RNases are primarily of the T1 and T2 families (MacIntosh, 2011).

To surmount this complication, we adapted a column-based method to purify fungal T1 and T2 RNases by binding them to an agarose column coupled with guanosine monophosphate (GMP) (Fields et al., 1971). We found that cell wall digesting enzymes readily passed through

GMP columns, while the contaminating RNases remained stuck to the column. After column depletion, RNase activity was almost completely removed from the enzyme blend (Figure 2C). Purified enzymes were stable when stored in glycerol stocks for at least a year, and so purification did not need to be performed repeatedly.

RNA quality after high temperature digestion

We tested the effect of the fixed tissue dissociation procedure on RNA quality. RNA isolated from fixed anthers had an average RNA Integrity Number (RIN) of 9.3 demonstrating fixation did not cause any significant decrease in RNA quality (Figure 2D). Fixed anthers digested at 50°C in a commercial enzyme blend had a RIN of 4.1 with very noticeable loss of ribosomal RNA. After fixation then digestion with purified enzymes, the RIN was 6.7 demonstrating the tissue dissociation protocol can produce RNA of reasonable quality, although it does produce a decrease in RNA integrity relative to undigested tissue. When fixed anthers were incubated in enzyme buffer at 50°C without enzymes, we observed a similar RIN of 6.1. Therefore, the decrease in RNA integrity during incubation is not enzyme dependent, rather we suspect this degradation is caused by endogenous anther RNases that survive the fixation process. Future improvements of the method may be able to inhibit residual tissue RNases.

Cell type identification

We next tested whether single cells isolated from fixed dissociated anthers had sufficient RNA quality for scRNA-Seq. We sequenced four libraries of 96 single cells each, two using a BioSorter (Union Biometrica) and two using a Hana (Namocell) to sort and isolate single cells. Of the 384 possible single cell samples, 307 had more than 500 UMIs and 200 genes detected after removal of cell-cycle genes. We detected an average of 5,885 UMIs and 2,016 genes per cell. The dataset was classified into four distinct clusters, two of which were subset and reclustered based on marker gene expression to produce six total clusters (Figure 3). The total number of UMIs did not vary between the six cell clusters (Supplemental Figure 2); furthermore, two independent scRNA-seq experiments using different cell sorting platforms each contributed to the different clusters, indicating that the cell clustering was reproducible between replicates (Supplemental Figure 2B).

We next asked if we could associate the cell clusters with established anther cell types based on known marker genes and gene expression of anther cell types isolated by laser capture micro-dissection (LCM) (Zhou et al., 2021). We observed a strong correlation between the genes expressed in cluster 6 and genes expressed in tapetal cells by LCM (Figure 3B; Supplemental Figure 2C). Cluster 6 further expressed several male-sterility genes known to be up-regulated in the tapetum: *basic Helix-Loop-Helix 51* (*bHLH51*), *Male-sterile 8* (*Ms8*), and *Male-sterile 44* (*Ms44*) (Nan et al., 2017; Wang et al., 2010; Fox et al., 2017) (Figures 3, C-E; Supplemental Figure 3). Genes expressed in cluster 5 were highly correlated with the LCM meiocyte sample and also had strong expression of genes known to be highly expressed in meiocytes: *Trehalose 6-Phosphate Phosphatase* (*Trps8*), *C3H Transcription Factor 33* (*C3H3*), and a *Small Heat Shock Protein* (*sHSP*) (Nelms and Walbot, 2019; Zhou et al., 2021) (Figure 3, F-I; Supplemental Figures 2D, 3, D-F). Based on these data, we conclude that cluster 6 contains tapetal cells and cluster 5 contains meiocytes.

The remaining cell clusters all showed low correlation with the LCM tapetal and meiocyte samples but high correlation with the LCM other somatic cells (epidermis, endothecium, middle layer) sample (Figure 4; Supplemental Figure 2E). Beyond the tapetum, the maize anther contains multiple different somatic cell types including middle layer, endothecium, epidermis, connective, and vasculature. There is no expression data for these anther cell types and so we attempted to associate the remaining clusters to cells based on knowledge of anther cell biology. Murphy *et al.*, (2015) discovered that the endothecium contains significantly more functioning chloroplasts than the other anther cell layers. We found plastid transcripts were generally expressed in cluster 1 much higher than all other clusters (Figure 4B; Supplemental Figure 2F). Furthermore, the photosynthesis-associated genes from Murphy *et al.,* (2015) and nuclear-encoded chloroplastic genes (PantherDB Family #21649) (Mi et al., 2021) were selectively expressed in cluster 1 (Figures 4, C-E; Supplemental Figures 3, G-I). Thus, we associate cluster 1 with the endothecium.

The anther epidermis produces cuticular waxes to seal and protect the maize anther from the environment. These waxes are formed by converting C_2 acetyl-coenzyme A (acetyl-CoA) into C_{16} or C_{18} fatty acids then further converted into fatty acyl-CoAs by long-chain acyl-CoA synthetases (LACS); these are remodeled and extended into C_{24} to C_{34} fatty acids, or very-long-chain fatty acids (VLCFAs) (Zheng et al., 2019; Schnurr et al., 2004). A number of genes have

been found to regulate the production of theses epicuticular waxes in maize, rice, and Arabidopsis (Zheng et al., 2019; Jung et al., 2006; Schnurr et al., 2004). We focused on *Glossy14*, the maize homolog of rice *Wax-Deficient Anther1* (*Wda1*), and the maize homolog of Arabidopsis *LACS2* – mutations in these three genes have been shown to result in significantly decreased epicuticular wax load (Zheng et al., 2019; Jung et al., 2006; Schnurr et al., 2004). We found that cluster 2 had the highest average expression levels and proportion of cells expressing these genes, suggesting cluster 2 contains epidermal cells (Figures 4, F-H; Supplemental Figures 3, J-L).

The final two clusters were unidentifiable as little is known about the genetic activity of the remaining somatic cell types: the middle layer, connective cells, and vasculature. However, we were able to generate a list of the most specifically expressed genes for each cluster, providing a putative list of marker genes (Figure 5). The majority of these genes are unannotated, but the cell types that these genes are expressed in can be determined using RNA *in situ* hybridization, LCM RNA-seq, or scRNA-seq accompanied by cell imaging. Additionally, scRNA-seq of a full developmental time course could readily connect known cell type precursors and their derivative cell types, such as the secondary parietal cells differentiating into the tapetum and middle layer. We were also able to identify modules of co-regulated genes specific to each cluster (Figure 5B). Cluster-specific modules can be analyzed for gene ontology (GO) term enrichment providing insight into the biological processes, cellular component, and molecular function and of each module. For example, Module 31, which was highly up-regulated in the endothecium cluster, is highly enriched for genes relating to photosynthesis and localized in the chloroplast (Figure 5C). Similar analyses can be utilized to verify cluster identification or further narrow down the cell type identity of unknown clusters.

DISCUSSION

Difficulties in the dissociation of tissues and isolation of single cells has restricted plant single-cell RNA-sequencing to only the most researched plant species and tissues. We provide a scRNA-seq protocol that can be readily adapted to an array of plant taxa and tissues, spanning well beyond typical model plant species and tissues. By incorporating cellular fixation and enzymes purified of RNases, we demonstrated that this fixation-based protocol had a significantly higher and more uniform cell release than well-established fresh protoplasting

protocols in multiple tissues and species while maintaining high quality RNA with minimal to no additional optimization. Fixation stabilizes the cells making them more resistant to mechanical force and permitting the use of increased digestion temperatures relative to highly fragile and environmentally sensitive fresh protoplasts. This protocol is highly scalable, permitting the isolation and sequencing of a few cells isolated by hand to thousands of cells isolated and dispensed with a cell sorter.

With any new method, it is important to consider potential limitations. The advantage of our method is that it allows drastically better release of complete cells from plant tissues. However, there are some contexts where this method has drawbacks. First, some plant cells have large fluid filled vacuoles and are very fragile after fixation; for instance, we found maize leaf mesophyll cells do not hold up well to our method. As a result, other approaches may be better for cells with very high water content. With any new tissue, we recommend first testing this method using commercially available enzymes to see how well the cells of interest are successfully released before committing to enzyme purification.

Second, we suspect the method will not be compatible with widely used droplet-based technologies such as 10X Genomics. This is because the large size and unusual shape of many plant cells (10 - 100 µm) relative to animal cells (10 - 30 µm) might result in clogging the flow cells used for droplet-based scRNA-seq. Fortunately, we identified two technologies for isolating large plant cells in high-throughput.

We found the BioSorter (Union Biometrica, Inc.) and Hana (Namocell) can readily sort and dispense single plant cells into plates for library preparation. In addition, SPLiT-seq (Rosenberg et al., 2018), a relatively new and inexpensive ways to construct scRNA-seq libraries, requires fixed cells and might work smoothly with our tissue dissociation method.

We were able to putatively identify four clusters as the tapetum, epidermis, endothecium, and meiocytes based on a few known cell type marker genes and the established biology of specific cell types. The remaining clusters likely consist of the middle layer, vascular, and connective cells, but little is known about the expression patterns of these somatic cell types. For example, the function of the middle layer is completely unknown, although its developmental origin and fate are well-established in maize. This ephemeral cell layer differentiates from the secondary parietal cells along with the tapetum early in anther development then undergoes programmed cell death prior to the completion of meiosis. A few male-sterile maize mutants

have aberrant middle layer phenotypes, however, the cell layer has been largely understudied relative to the tapetum (Walbot and Egger, 2016). Targeted analysis of this enigmatic cell layer using scRNA-seq could reveal its function and activity in the anther.

It is entirely possible that unknown cell types exist among the vascular and connective tissues or even among the primary four somatic layers of the anther, as demonstrated by Murphy et al., (2015) with the subclassification of the endothecium into the subepidermal endothecium and interendothecium, the endothecial cells adjacent to the connective tissue. In addition, maize tapetal cells asynchronously become binucleate throughout meiosis, suggesting a key developmental transition in this cell type when anthers are 2.0 mm in length. The substructure of the tapetal cluster may reflect this cellular change or the binucleate tapetal cells could be clustered in the unidentified clusters. Increased sampling and the incorporation of developmental trajectories would heighten the resolution of each cell cluster revealing unknown and unresolved cell types.

The *de novo* identification of the top specific marker genes and co-regulated gene modules for each cluster can help elucidate the identity of unknown scRNA-seq cell clusters. RNA *in situ* hybridization of these putative marker genes could locate these cells within the maize anther, while LCM RNA-seq of the known cell layers could serve as a background reference. GO term enrichment analyses of the co-regulated gene modules can provide critical insight into the function and biology of unknown cell clusters. Coupled with scRNA-seq, high-throughput cell imaging of each fixed cell before library preparation can aid in the categorization of cells based on cell size, shape, and organellar composition, traits that differ considerably among plant cell types but that are eliminated by the protoplasting of fresh cells.

Single-cell RNA-seq has revolutionized our understanding of animal cell identification, development, and evolution over the last two decades while scRNA-seq in plants has been slow to develop, largely due to the extensive optimization required for dissociating and isolating plant cells. This fixation-based cell dissociation protocol coupled with scRNA-seq should similarly open the door to such discoveries for plant research regardless of species or tissue.

METHODS

Plant growth and anther dissection

Zea mays (inbred line W23 *bz2*) individuals were grown under greenhouse conditions in Stanford, CA, USA with 14-h day/10-h night lighting. Daily irrigation and fertilization were maintained for robust growth. Beginning five to six weeks after planting, individual plants were felled ~20 cm above ground level for anther dissection between 8:00 and 9:00 am. The sacrificed plants were taken to the lab within 10 min where the tassels were dissected out of the stem and leaf whorl. A Leica M60 dissecting scope (Leica Microsystems Inc.) and stage micrometer (Fisher Scientific) were used to isolate 2.0 mm anthers from the upper florets of spikelets along the central spike of the tassel.

Cellular release

Cell release of fixed and fresh maize anthers was compared in a variety of conditions. Three 2.0 mm anthers were pooled per replicate with five replicates per condition. Fresh anthers were digested at 30°C for 90 min or 16 h in the enzyme mix from Nelms & Walbot (2019). Fixed samples were left in ice-cold Farmer's solution (3:1 100% ethanol:glacial acetic acid) for two h, washed twice in ice-cold 0.1X phosphate-buffered saline (PBS; Sigma-Aldrich) for five min, then digested at 30°C or 50°C for 90 min in 20 mM MES, pH 5.7 with a 1:10 dilution of purified cell wall digesting enzyme stock (enzymes were stored in glycerol stocks, see below; stocks were normalized so that a 1:10 dilution has the same A280 as a 1.25% w/v Cellulase-RS and 0.4% w/v Macerozyme-R10 solution). The cells from the digested, fixed anthers were dissociated via shear force between two microscope slides with thin tape as a spacer. For each replicate, the number of single cells was estimated using a hemocytometer then averaged. Images of the dissociated cells were taken on a Nikon Diaphot inverted microscope with a mounted Nikon D40 camera.

Cell release from maize root tips was compared in three conditions: fresh protoplasting following Ortiz-Ramirez *et al.* 2018, fixation and digestion with the enzyme concentrations from Ortiz-Ramirez *et al*. 2018, or fixation and digestion with our highly reduced enzyme mix. Maize seeds were treated, germinated, and grown following Ortiz-Ramírez *et al.* (2018). Seedling primary roots were cut 5 mm above the tip with a scalpel. Three root tips were pooled per replicate with five replicates per condition. Fresh root tips were pre-treated, washed, digested in

enzyme (1.2% Cellulase-RS, 0.36% Pectolyase Y-23, 0.4% Macerozyme-R10, 1.2% Cellulase-R10; Sigma Aldrich; Yakult Pharmaceutical Industry Co.), filtered, and washed. The fresh protoplasts were counted with a hemocytometer. The fixed samples were left in ice-cold Farmer's solution for two h, washed twice with ice-cold 0.1X PBS for five min then digested at 50°C with the enzyme mix from Ortiz-Ramírez *et al.* (2018) or the enzyme mix from this protocol. Digested tissue was manually disrupted with pipetting, then the number of individual cells counted with a hemocytometer.

To test the applicability of our fixation protocol to non-model plant tissues, the cell release from leaf tissues of two basal angiosperms, *Amborella trichopoda* and waterlily (*Nymphaea colorata*), were imaged following fixation and digestion as previously described.

Enzyme purification

RNase present in fungal cell wall digesting enzymes were depleted by passing concentrated enzyme solution through agarose beads coupled with guanosine monophosphate (GMP). GMP beads were prepared using the procedure from Kanaya & Uchida (1981), with modifications: 50 mL suspended ω-aminohexyl–agarose beads (Sigma-Aldrich) were washed three times in water and then three times in 0.1M borax, pH 9.0 (Sigma-Aldrich). Meanwhile, sodium metaperiodate (Chem-Impex) was dissolved in 6 mL water to a final concentration of 0.2 M, and 488 mg guanosine monophosphate was added; the solution was incubated at room temperature (RT) in the dark for 1 h with gentle mixing. The washed agarose beads were resuspended in 0.1 M borax, pH 9.0 to a total volume of 36 mL, then the 6 mL solution containing oxidized GMP was added and the reaction was incubated at RT with gentle mixing for 2-4 h. Finally, 136 mg of solid sodium borohydride (Sigma-Aldrich) was slowly added to the reaction and the solution was gently mixed at 4°C for 1 h with the cap loosened to allow ventilation. The coupled GMP beads were washed three times each with 0.1 M borax, then water, then 1 M sodium chloride. Washed beads were loaded into a cleaned out Superdex 200 10/300 FPLC column (Cytiva) and stored in 1 M sodium chloride until further use. Remaining beads were stored in a sealed container in 1 M sodium chloride until further use.

For purification, the enzymes were resuspended at 10X concentration (12.5% w/v Cellulase-RS and 4% w/v Macerozyme R10) in RNase binding buffer (RBB; 150 mM NaCl, 10 mM citrate, pH 7.0). Four mL of GMP beads were loaded in a Kontes Flex-Column (Kimble

Chase) gravity flow column and equilibrated with RBB at 4°C, then the enzyme mix was passed through this column. The flow through was collected and then run through the pre-equilibrated GMP-agarose FPLC column at 4°C using a peristaltic pump. Fractions were collected and those with >0.1 absorbance at A280 were pooled. Pooled enzymes were concentrated using an Amicon Ultra-15 Centrifugal Filter Unit, MWCO 30 kDa (MilliporeSigma) at 4°C until a 1:10 dilution of the enzyme blend had 0.75 absorbance at A280. The Amicon concentrators were made using regenerated cellulase esters and the concentrated enzyme blend was capable of weakening these membranes; for future purifications, it is recommended to use a centrifugal concentrator with a membrane made from a different material. Concentrated enzymes were mixed 1:1 with glycerol and stored at -20°C until further use. For digestions, enzyme stocks were used at 1/10th the final volume. RNase activity in the purified and unpurified enzyme mix was quantified using the Ambion RNaseAlert Lab Test Kit (Invitrogen).

RNA integrity

Anther RNA quality was tested in three conditions of cell preparation: 1) fixed in Farmer's solution then washed twice in 0.1X PBS then flash frozen, 2) fixed, washed, and digested in commercial enzyme, and 3) fixed, washed, and digested in purified enzyme. For each condition, 2.0 mm anthers were isolated from five separate plants with ten anthers pooled per plant. The flash frozen samples were homogenized via bead beating in a 2000 Geno/Grinder (SPEX CertiPrep) with baked 4 mm steel balls. The fixed samples were left in ice-cold Farmer's solution for two h, washed twice in ice-cold 0.1X PBS for five min, then incubated at 50°C for 90 min with purified or commercial enzyme (1.25% w/v Cellulase-RS and 0.4% w/v Macerozyme R10). The RNeasy Plant Mini Kit (Qiagen) was used to extract RNA from samples via the standard protocol. RNA was quality-checked on an Agilent 2100 BioAnalyzer with the RNA 6000 Nano assay (Agilent Technologies). The RNA Integrity Number (RIN) for the five replicates of each condition were averaged and reported alongside the error.

Fixed cell isolation for scRNA-Seq

Anthers from four individuals of wild-type (W23) maize were dissected out. One of the three anthers per floret was used for imaging on a Nikon Diaphot inverted microscope with a Nikon D40 mounted camera at 10X magnification. The remaining two anthers per floret were fixed in

387 ice-cold Farmers solution for two h, washed twice for 5 min in 0.1X PBS, and then one anther
388 was digested for 90 min at 50°C in the purified enzyme mix while the other anther was saved at -
389 20°C. Following digestion, shear force was applied to the anther between two microscope slides
390 with thin tape on each end to prevent the anther from being fully crushed. The top microscope
391 slide was slid back and forth 5-10 times and the sample checked under the dissecting scope to
392 ensure separation of the fixed cells. The cells were washed from the slides into 1 mL of cold
393 0.1X PBS via pipette and stained with SYBR Green I nucleic acid gel stain (Invitrogen) for 20
394 min. The cells were then filtered through a 100 µm (if bound for the BioSorter) or 40 µm (if
395 bound for the Hana) nylon cell strainer (Corning Inc.) into 50 mL Falcon tubes. The stained cells
396 were then sorted into 384-well plates or 96-well plates, each well containing 0.8 µL Primer
397 Master Mix (0.225% Triton X-100, 1.6 mM dNTP mix, 1.875 uM barcoded oligo[dT] CEL-seq2
398 primers; Sigma-Aldrich, New England Biolabs) using a BioSorter (Union BioMetrica) or Hana
399 Single Cell Dispenser (Namocell). Following cell sorting, the plates were spun at 400 x *g* then
400 stored at -80°C.
401
402 **CEL-Seq2 library preparation**
403 Single cell libraries were prepared following the CEL-seq2 protocol (Hashimshony et al., 2016)
404 with alterations similar to Nelms & Walbot (2019). The samples were thawed then incubated at
405 65°C for 3 min, spun, then incubated again at 65°C for 3 min then placed on ice. To each sample
406 0.7 µL of reverse transcription mix (8:2:1:1 of Superscript IV 5X Buffer, 100 mM DTT, RNase
407 Inhibitor, Superscript IV; ThermoFisher Scientific) was added, spun down, then incubated at
408 42°C for 2 min, 50°C for 15 min, 55°C for 10 min then placed on ice. The samples were pooled
409 by row into 8-strip tubes and excess primers were digested with the addition of 4.6 µL
410 exonuclease I mix (2.5 µL of 10X Exonuclease I Buffer, 2.1 µL Exonuclease I; New England
411 Biolabs) then incubated at 37°C for 20 min, 80°C for 10 min then placed on ice. To each of the
412 pooled samples 44.28 µL (1.8X volume) of pre-warmed RNAClean XP beads was added and
413 mixed well via pipette. The samples were left to incubate at RT for 15 min then placed on a
414 magnetic rack until the liquid became clear. The supernatant was carefully pipetted out, making
415 sure not to disturb the beads, and discarded. The beads were washed twice with 100 µL of
416 freshly prepared 80% ethanol. The ethanol was pipetted out then the beads were left to dry for 5

417 min. The RNA was eluted from the beads with 7 µL RNase-free water and incubated for two
418 minutes at RT then mixed via pipette.
419 Second strand synthesis was initiated with the addition of 3 µL second strand synthesis
420 mix (2.31 µL Second Strand Reaction dNTP-free Buffer, 0.23 µL 10 mM dNTPs, 0.08 µL DNA
421 ligase, 0.3 µL DNA polymerase I, 0.08 µL RNase H; New England Biolabs) and then incubated
422 at 16°C for 4 h. Samples were further pooled into a single tube and 30 µL Ampure XP beads
423 (Beckman Coulter Life Sciences) with 66 µL bead binding buffer (2.5 M NaCl, 20% PEG 8000;
424 Sigma-Aldrich) (1.2X volume) was added. The sample was incubated for 15 min at RT then
425 washed and dried as described for the RNAClean XP beads above. The RNA was eluted from
426 the beads with 6.4 µL of RNase-free water, left to incubate for 2 min at RT, and mixed via
427 pipette.
428 *In vitro* transcription was initiated with the addition of 9.6 µL of MegaScript T7 IVT mix
429 (1:1:1:1:1:1 of CTP solution, GTP solution, UTP solution, ATP solution, 10X Reaction Buffer,
430 T7 Enzyme Mix; ThermoFisher Scientific) to the sample then incubated at 37°C overnight. The
431 beads were removed from the sample with a magnetic rack and 28.8 µL (1.8X volume) of pre-
432 warmed RNAClean XP beads (Beckman Coulter Life Sciences) was added then incubated at RT
433 for 15 min then washed and dried as described above. Once dry, 6.5 µL of RNase-free water was
434 added to the beads, incubated for 2 min at RT, and mixed via pipette. The amplified RNA quality
435 and quantity were analyzed with an RNA Pico 6000 chip on an Agilent 2100 BioAnalyzer
436 (Agilent Technologies).
437 To the samples 1.5 µL of priming mix (9:5:1 of RNase-free water, 10 mM dNTPs, 1M
438 tagged random hexamer primer: 5'-GCCTTGGCACCCGAGAATTCCANNNNNN) was added
439 and incubated at 65°C for 5 min then placed on ice. A second round of reverse transcription was
440 initiated with the addition of 4 µL of reverse transcription mix (4:2:1:1 of First Strand Buffer, 0.1
441 M DTT, RNaseOUT, SuperScript II; ThermoFisher Scientific) to each sample then incubated at
442 25°C for 10 min, 42°C for 1 h, and 70°C for 10 min before being placed on ice. For the final
443 PCR, 5.5 µL of sample were added to 21 µL of PCR master mix with Illumina TruSeq Small
444 RNA PCR primer (RP1) and Index Adaptor (RPI "X") (6.5 µL RNase-free water, 12.5 µL Ultra
445 II Q5 Master Mix, 1 µL of 10 µM RP1, 1 µL of 10 µM RPI "X"). Libraries were amplified with
446 13 rounds of PCR (98°C for 30 sec, then 13 cycles of 98°C for 10 sec, 65°C for 15 sec, and 72°C
447 for 30 sec and finished with 72°C for 3 min). The final PCR products were purified with 26.5 µL

(1.0X volume) of Ampure XP beads (Beckman Coulter Life Sciences) then incubated at RT for 15 min then washed and dried as described above. The cDNA was eluted from the beads with 25 µL RNase-free water and purified again with 25 µL (1.0X volume) of Ampure XP beads (Beckman Coulter Life Sciences) then incubated at RT for 15 min then washed and dried as described above. The final purified libraries were eluted into 10 µL RNase-free water incubated for 2 min at RT and mixed via pipette. The cDNA was then assessed with an Agilent BioAnalyzer High Sensitivity DNA chip.

Two libraries of 96 cells isolated with the BioSorter were sequenced on a HiSeqX and two libraries of 96 cells isolated with the Hana were sequenced on a NovoSeq (Illumina) at Novogene Co. (Sacramento, CA, USA) with paired-end 150 base-pair (bp) reads. Primer sequences can be found in Table S1-2. All primers were synthesized by the Stanford Protein and Nucleic Acid Facility (PAN, Stanford University, Stanford, CA, USA). Detailed step-by-step protocols of enzyme purification, fixed cell isolation, and library preparation can be found in the Supplementary Materials.

Read filtering, mapping, and initial processing

Paired-end raw reads were demultiplexed based on cell-specific barcodes (Table S1) using Fastq-Multx (Aronesty, 2013). The UMI sequences from read 1 were added to the read 2 sequence names and then filtered and trimmed with Fastp (parameters: -y -x -3 -f 6) (Chen et al., 2018). The clean reads were mapped to the B73 reference genome (AGP v. 4) (Jiao et al., 2017) with HiSat2 (Kim et al., 2019), and unique molecular identifiers (UMIs) quantified with SAMtools (Li et al., 2009)and UMI-tools (Smith et al., 2017). Cell cycle heterogeneity has been shown to distort the clustering of cells, thus all cell-cycle genes from Nelms & Walbot (2019) were removed and cells with fewer than 500 UMIs or 200 genes detected were discarded. Genes that were detected in fewer than 3 cells were also discarded.

To initially compare our dataset with that of known cell types we assessed the similarity of our data with laser-capture microdissection (LCM) sequencing data of known cell types and whole anthers from Zhou et al. (2021), which were also prepared from 2.0 mm W23 maize anthers using the same CEL-Seq2 library preparation. We normalized our UMIs into transcripts per million (TPM) and log transformed after adding a pseudocount of 100. We then subtracted the single cell TPMs by the log transformed TPMs of the whole anthers to produce ratio

measurements. The LCM data had samples for tapetal, meiocyte, and other somatic (middle layer, endothecium, epidermis) cell types and were similarly processed relative to the whole anther data. We then calculated the cell-to-cell Pearson's correlations of all our single cells relative to each of the LCM samples.

Cell clustering and cell type identification

Cell clustering and cell type analyses were performed using Monocle 3 (Cao et al., 2019) in R/RStudio (R Core Team, 2013; Team, 2015). The UMI counts were normalized via log and size factor with an added pseudocount of 1 and dimensionality reduced via Principal Component Analysis (PCA) consisting of 10 principal components based on the leveling point of an elbow plot of the percentage of variance explained by ranked principal components. Batch effects were removed with the align_cds function in Monocle. Clusters were determined and visualized with Uniform Manifold Approximation and Projection (UMAP) with a resolution of 0.01(McInnes et al., 2020). Correlation values of each cell with the LCM tapetal, meiocyte, and other somatic cell types were mapped onto the UMAP, as well as the percentages of transcripts from the plastid genome and mitochondrial genome. The meiocyte cluster was manually separated from the endothecium cluster based on the LCM correlation data and meiocyte marker genes; it is likely that Monocle did not separate these clusters due to the scarcity of meiocyte cells despite the clear separation in the UMAP. The other somatic 1 (OS1) cluster was subset and reclustered to identify and separate the epidermis cluster based on putative marker genes of the known biology of the cell type (Table 1).

De novo cluster specific marker genes were identified and ranked using pseudo R^2 values from the marker_test_res function in Monocle. Co-regulated genes were grouped into modules by using the graph_test function to calculate Moran's I for each gene then applying the Louvian community analysis with a resolution of 0.01 via the find_gene_modules function. We then plotted the aggregate expression of all genes per module for each UMAP cluster to identify cluster-enriched gene modules. The genes from these cluster-enriched modules were then extracted and analyzed for gene ontology (GO) term enrichment relative to the Maize AGPv.4 reference in AgriGO v2(Tian et al., 2017).

Data availability

Sequencing data are deposited in the NCBI Gene Expression Omnibus under BioProject PRJNA760550.

ACKNOWLEDGMENTS

This work was supported by the National Science Foundation awards 1907220 (to DBM) and 17540974 (to B. C. Meyers and V.W.). We thank Ed Buckler for sequencing of the preliminary libraries.

AUTHOR CONTRIBUTIONS

DBM and BN performed most experiments and designed the study. BN designed and optimized the enzyme purification protocol. DBM analyzed the RNA-seq data. DBM wrote the manuscript with input from BN and VW.

COMPETING INTERESTS

A patent on the enzyme purification protocol has been filed by Stanford University with BN as inventor (U.S. Patent Application No. 17/196,681).

527 **LITERATURE CITED**

528 Aronesty, E. (2013). Comparison of sequencing utility programs, Open Bioinf. J 7: 1–8.

529 Cao, J., Spielmann, M., Qiu, X., Huang, X., Ibrahim, D.M., Hill, A.J., Zhang, F., Mundlos, S.,
530 Christiansen, L., and Steemers, F.J. (2019). The single-cell transcriptional landscape of
531 mammalian organogenesis. Nature 566: 496–502.

532 Chaubal, R., Zanella, C., Trimnell, M.R., Fox, T.W., Albertsen, M.C., and Bedinger, P. (2000).
533 Two male-sterile mutants of *Zea mays* (Poaceae) with an extra cell division in the anther
534 wall. Am. J. Bot. 87: 1193–1201.

535 Chen, S., Zhou, Y., Chen, Y., and Gu, J. (2018). fastp: an ultra-fast all-in-one FASTQ
536 preprocessor. Bioinformatics 34: i884–i890.

537 Conde, D., Triozzi, P.M., Balmant, K.M., Doty, A.L., Miranda, M., Boullosa, A., Schmidt,
538 H.W., Pereira, W.J., Dervinis, C., and Kirst, M. (2021). A robust method of nuclei isolation
539 for single-cell RNA sequencing of solid tissues from the plant genus *Populus*. PLoS One
540 16: e0251149.

541 Denyer, T., Ma, X., Klesen, S., Scacchi, E., Nieselt, K., and Timmermans, M.C.P. (2019).
542 Spatiotemporal developmental trajectories in the Arabidopsis root revealed using high-
543 throughput single-cell RNA sequencing. Dev. Cell 48: 840-852.e5.

544 Fields, R., Dixon, H.B., Law, G.R., and Yui, C. (1971). Purification of ribonuclease T 1 by
545 diethylaminoethylcellulose chromatography. Biochem. J. 121: 591–596.

546 Fox, T., DeBruin, J., Haug Collet, K., Trimnell, M., Clapp, J., Leonard, A., Li, B., Scolaro, E.,
547 Collinson, S., and Glassman, K. (2017). A single point mutation in Ms44 results in
548 dominant male sterility and improves nitrogen use efficiency in maize. Plant Biotechnol. J.
549 15: 942–952.

550 Han, X. et al. (2020). Construction of a human cell landscape at single-cell level. Nature 581:
551 303–309.

552 Hashimshony, T., Senderovich, N., Avital, G., Klochendler, A., de Leeuw, Y., Anavy, L.,
553 Gennert, D., Li, S., Livak, K.J., and Rozenblatt-Rosen, O. (2016). CEL-Seq2: sensitive
554 highly-multiplexed single-cell RNA-Seq. Genome Biol. 17: 77.

555 Jean-Baptiste, K., McFaline-Figueroa, J.L., Alexandre, C.M., Dorrity, M.W., Saunders, L.,
556 Bubb, K.L., Trapnell, C., Fields, S., Queitsch, C., and Cuperusa, J.T. (2019). Dynamics of
557 gene expression in single root cells of *Arabidopsis thaliana*. Plant Cell 31: 993–1011.

558 Jiao, Y. et al. (2017). Improved maize reference genome with single-molecule technologies.
559 Nature 546: 524–527.
560 Jung, K.-H., Han, M.-J., Lee, D., Lee, Y.-S., Schreiber, L., Franke, R., Faust, A., Yephremov, A.,
561 Saedler, H., Kim, Y.-W., Hwang, I., and An, G. (2006). Wax-deficient anther1 is involved
562 in cuticle and wax production in rice anther walls and is required for pollen development.
563 Plant Cell 18: 3015–3032.
564 Kanaya, S. and Uchida, T. (1981). Purification of ribonuclease T1 by affinity chromatography. J.
565 Biochem. 89: 591–597.
566 Kanton, S. et al. (2019). Organoid single-cell genomic atlas uncovers human-specific features of
567 brain development. Nature 574: 418–422.
568 Kelliher, T. and Walbot, V. (2011). Emergence and patterning of the five cell types of the *Zea*
569 *mays* anther locule. Dev. Biol. 350: 32–49.
570 Kim, D., Paggi, J.M., Park, C., Bennett, C., and Salzberg, S.L. (2019). Graph-based genome
571 alignment and genotyping with HISAT2 and HISAT-genotype. Nat. Biotechnol. 37: 907–
572 915.
573 Li, H., Handsaker, B., Wysoker, A., Fennell, T., Ruan, J., Homer, N., Marth, G., Abecasis, G.,
574 and Durbin, R. (2009). The sequence alignment/map format and SAMtools. Bioinformatics
575 25: 2078–2079.
576 Lim, B., Lin, Y., and Navin, N. (2020). Advancing Cancer Research and Medicine with Single-
577 Cell Genomics. Cancer Cell 37: 456–470.
578 Liu, Q., Liang, Z., Feng, D., Jiang, S., Wang, Y., Du, Z., Li, R., Hu, G., Zhang, P., Ma, Y.,
579 Lohmann, J.U., and Gu, X. (2021). Transcriptional landscape of rice roots at the single-cell
580 resolution. Mol. Plant 14: 384–394.
581 Lopez-Anido, C.B., Vatén, A., Smoot, N.K., Sharma, N., Guo, V., Gong, Y., Anleu Gil, M.X.,
582 Weimer, A.K., and Bergmann, D.C. (2021). Single-cell resolution of lineage trajectories in
583 the Arabidopsis stomatal lineage and developing leaf. Dev. Cell 56: 1043-1055.e4.
584 MacIntosh, G.C. (2011). RNase T2 Family: enzymatic properties, functional diversity, and
585 evolution of ancient ribonucleases BT - Ribonucleases. In A.W. Nicholson, ed (Springer
586 Berlin Heidelberg: Berlin, Heidelberg), pp. 89–114.
587 McInnes, L., Healy, J., and Melville, J. (2020). UMAP: uniform manifold approximation and
588 projection for dimension reduction.

Mi, H., Ebert, D., Muruganujan, A., Mills, C., Albou, L.-P., Mushayamaha, T., and Thomas, P.D. (2021). PANTHER version 16: a revised family classification, tree-based classification tool, enhancer regions and extensive API. Nucleic Acids Res. 49: D394–D403.

Nan, G., Zhai, J., Arikit, S., Morrow, D., Fernandes, J., Mai, L., Nguyen, N., Meyers, B.C., and Walbot, V. (2017). MS23 , a master basic helix-loop-helix factor , regulates the specification and development of the tapetum in maize.: 163–172.

Nelms, B. and Walbot, V. (2019). Defining the developmental program leading to meiosis in maize. Science (80-.). 364: 52–56.

Ortiz-Ramírez, C., Arevalo, E.D., Xu, X., Jackson, D.P., and Birnbaum, K.D. (2018). An efficient cell sorting protocol for maize protoplasts. Curr. Protoc. plant Biol. 3: e20072.

Paik, D.T., Cho, S., Tian, L., Chang, H.Y., and Wu, J.C. (2020). Single-cell RNA sequencing in cardiovascular development, disease and medicine. Nat. Rev. Cardiol. 17: 457–473.

Pardo, A.G. and Forchiassin, F. (1999). Influence of temperature and pH on cellulase activity and stability in Nectria catalinensis. Rev. Argent. Microbiol. 31: 31–35.

R Core Team (2013). R: A language and environment for statistical computing.

Rosenberg, A.B. et al. (2018). Single-cell profiling of the developing mouse brain and spinal cord with split-pool barcoding. Science (80-.). 360: 176–182.

Ryu, K.H., Huang, L., Kang, H.M., and Schiefelbein, J. (2019). Single-cell RNA sequencing resolves molecular relationships among individual plant cells. Plant Physiol. 179: 1444–1456.

Schnurr, J., Shockey, J., and Browse, J. (2004). The acyl-CoA synthetase encoded by LACS2 is essential for normal cuticle development in Arabidopsis. Plant Cell 16: 629–642.

Seyfferth, C., Renema, J., Wendrich, J.R., Eekhout, T., Seurinck, R., Vandamme, N., Blob, B., Saeys, Y., Helariutta, Y., Birnbaum, K.D., and De Rybel, B. (2021). Advances and opportunities in single-cell transcriptomics for plant research. Annu. Rev. Plant Biol. 72: 847–866.

Smith, T., Heger, A., and Sudbery, I. (2017). UMI-tools: modeling sequencing errors in Unique Molecular Identifiers to improve quantification accuracy. Genome Res. 27: 491–499.

Sunaga-Franze, D.Y., Muino, J.M., Braeuning, C., Xu, X., Zong, M., Smaczniak, C., Yan, W., Fischer, C., Vidal, R., Kliem, M., Kaufmann, K., and Sauer, S. (2021). Single-nuclei RNA-sequencing of plant tissues. bioRxiv: 2020.11.14.382812.

Team, Rs. (2015). RStudio: integrated development for R. RStudio, Inc., Boston, MA URL http//www. rstudio. com 42: 84.

Thrupp, N., Frigerio, C.S., Wolfs, L., Skene, N.G., Fattorelli, N., Poovathingal, S., Fourne, Y., Matthews, P.M., Theys, T., and Mancuso, R. (2020). Single-nucleus RNA-Seq is not suitable for detection of microglial activation genes in humans. Cell Rep. 32: 108189.

Tian, T., Liu, Y., Yan, H., You, Q., Yi, X., Du, Z., Xu, W., and Su, Z. (2017). agriGO v2. 0: a GO analysis toolkit for the agricultural community, 2017 update. Nucleic Acids Res. 45: W122–W129.

Walbot, V. and Egger, R.L. (2016). Pre-meiotic anther development: cell fate specification and differentiation. Annu. Rev. Plant Biol. 67: 365–395.

Wang, D., Oses-Prieto, J.A., Li, K.H., Fernandes, J.F., Burlingame, A.L., and Walbot, V. (2010). The male sterile 8 mutation of maize disrupts the temporal progression of the transcriptome and results in the mis-regulation of metabolic functions. Plant J. 63: 939–951.

Zhang, T.Q., Xu, Z.G., Shang, G.D., and Wang, J.W. (2019). A single-cell RNA sequencing profiles the developmental landscape of Arabidopsis root. Mol. Plant 12: 648–660.

Zheng, J., He, C., Qin, Y., Lin, G., Park, W.D., Sun, M., Li, J., Lu, X., Zhang, C., and Yeh, C. (2019). Co-expression analysis aids in the identification of genes in the cuticular wax pathway in maize. Plant J. 97: 530–542.

Zhou, X., Huang, K., Teng, C., Batish, M., Meyers, B.C., and Walbot, V. (2021). 24-nt phasiRNAs move from tapetal to meiotic cells in maize anthers. bioRxiv: 2021.08.24.457464.

TABLES

Table 1. Marker genes and source.

Cell Type	Gene ID	Gene Name	Panther Family	Source
Tapetum	Zm00001d053895	*bHLH51*	TRANSCRIPTION FACTOR ABORTED MICROSPORES (PTHR31945:SF11)	Nan et al., 2017
Tapetum	Zm00001d012234	*Ms8*	BETA-1,3-GALACTOSYLTRANSFERASE 8-RELATED (PTHR11214:SF275)	Wang et al., 2010
Tapetum	Zm00001d052736	*Ms44*	NON-SPECIFIC LIPID-TRANSFER PROTEIN C4 (PTHR35501:SF7)	Fox et al., 2017
Endothecium	Zm00001d032197	*Cab*	CHLOROPHYLL A-B BINDING PROTEIN 4, CHLOROPLASTIC (PTHR21649:SF4)	
Endothecium	Zm00001d021435	*Lhcb2*	CHLOROPHYLL A-B BINDING PROTEIN 1, CHLOROPLASTIC (PTHR21649:SF108)	
Endothecium	Zm00001d000279	*Rbcl2*	RIBULOSE BISPHOSPHATE CARBOXYLASE LARGE CHAIN (PTHR42704:SF9)	Murphy et al., 2015
Epidermis	Zm00001d004198	*Gl14*	CASP-LIKE PROTEIN 2B1 (PTHR33573:SF30)	Zheng et al., 2018
Epidermis	Zm00001d014055	ZM-*wda1*	VERY-LONG-CHAIN ALDEHYDE DECARBONYLASE GL1-5 (PTHR11863:SF210)	Jung et al., 2006
Epidermis	Zm00001d053127	ZM-*Lacs2*	LONG CHAIN ACYL-COA SYNTHETASE 2 (PTHR43272:SF4)	Schnurr et al., 2004; Zhao et al., 2019
Meiocyte	Zm00001d039101	*C3h3*	PROTEIN TIS11 (PTHR12547:SF18)	Nelms & Walbot, 2019
Meiocyte	Zm00001d050069	*Trps8*	TREHALOSE 6-PHOSPHATE PHOSPHATASE (PTHR10788:SF24)	Nelms & Walbot, 2019
Meiocyte	Zm00001d044874	ZM-*sHSP*	SHSP DOMAIN-CONTAINING PROTEIN (PTHR46991:SF9)	Zhou et al., 2021

FIGURE LEGENDS

Figure 1. Overview of the fixation-based single-cell RNA-seq protocol and maize anther anatomy. (A) Step-by-step schematic of the protocol workflow. (B) Transverse section of the maize anther at the beginning of meiosis. (C) Percentage of each cell type per 2.0 mm maize anther based on cell counts from Kelliher & Walbot (2011). (D) Average dimensions for each cell type of the 2.0 mm maize anther from Kelliher & Walbot (2011). Cell types are color coded: orange is epidermis (EP); green is endothecium (EN); red is middle layer (ML); blue is tapetum (TAP); pink is meiocyte (M); white is vascular/connective.

Figure 2. Cellular release and RNA integrity of fresh and fixed protoplasting protocols. (A) Maize anthers were digested for 90 min or 16 h at 30°C following the Nelms and Walbot (2019) protoplasting protocol, and cell release quantified via hemocytometer (grey bars). Fixed maize anthers were digested for 90 min at 30°C and 50°C using the reduced enzyme mix and cell release similarly quantified (blue bars). (B) Cellular release of maize root tips comparing the optimized protoplasting protocol from Ortiz-Ramirez *et al.* (2018) and the fixation-based protocol. Maize root tips were digested following Ortiz-Ramírez *et al.* (2018) and cell release quantified via hemocytometer (grey bars). Maize root tips were fixed then digested at 50°C for 90 min using the Ortiz-Ramírez *et al.* (2018) protoplast enzyme mix and the reduced enzyme mix then cell release was similarly quantified (blue bars). (C) RNA degradation rate of commercial versus purified enzyme mix. (D) RNA quality of fixed maize anthers without any digestion, fixed maize anthers that were digested at 50°C for 90 min in enzyme buffer lacking enzymes, fixed maize anther that were digested at 50°C for 90 min using commercial enzyme mix, and fixed maize anthers that were digested at 50°C for 90 min using purified enzyme mix. Different letters denote statistically significant variation (Student's *t* test, $P < 0.05$) and error bars represent standard error.

Figure 3. Maize anther scRNA-seq of tapetum and meiocyte marker genes. (A) UMAP clustering of 307 cells from 2.0 mm maize anthers into six distinct clusters. (B) Correlation values of each cell with LCM tapetal data. (C-E) Expression values per maize anther cell of tapetal marker genes mapped onto the UMAP clusters. (F) Correlation values of each cell with

LCM meiocyte data. (G-I) Expression values per maize anther cell of meiocyte marker genes mapped onto the UMAP clusters.

Figure 4. Endothecium and epidermis marker gene expression in maize anther cells. (A) Correlation values of each cell with LCM other somatic cell types (middle layer, endothecium, epidermis) data. (B) Percentage of total UMIs originating from the plastid for each cell. (C-E) Expression values per maize anther cell of putative endothecium marker genes mapped onto the UMAP clusters. (F-H) Expression values per maize anther cell of putative epidermis marker genes mapped onto the UMAP clusters.

Figure 5. *De novo* marker gene identification and co-regulated gene modules. (A) Top three marker genes for each UMAP cluster with expression and percentage of cells from each cluster expressing the gene. (B) Co-regulated gene modules and expression scores for each UMAP cluster. (C) Gene ontology (GO) enrichment analysis of Module 31 sorted by biological processes (blue bars) and cellular component (green bars). Significantly enriched GO terms were selected based on a false discovery rate (FDR) < 0.05.

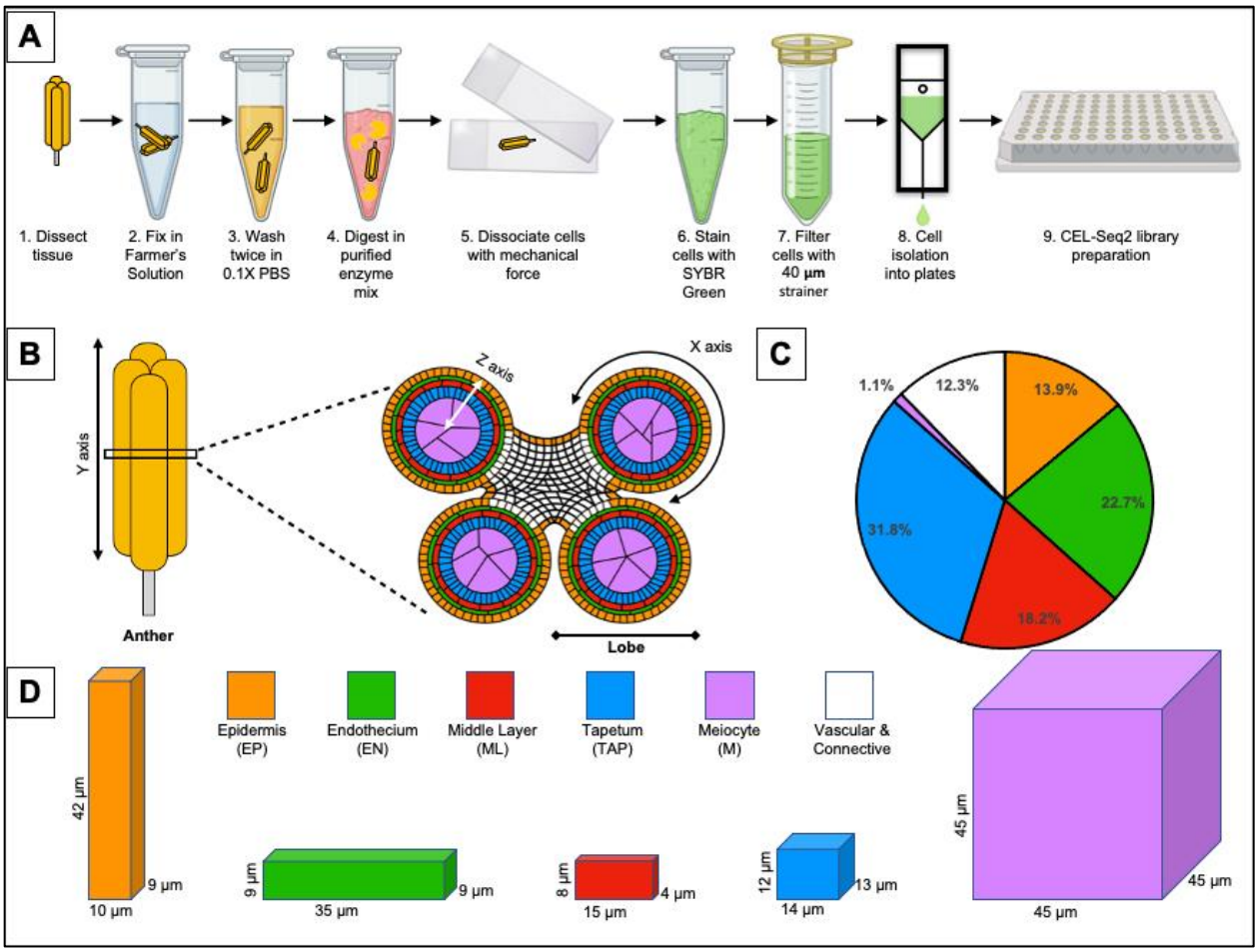

Figure 1. Overview of the fixation-based single-cell RNA-seq protocol and maize anther anatomy. (A) Step-by-step schematic of the protocol workflow. (B) Transverse section of the maize anther at the beginning of meiosis. (C) Percentage of each cell type per 2.0 mm maize anther based on cell counts from Kelliher & Walbot (2011). (D) Average dimensions for each cell type of the 2.0 mm maize anther from Kelliher & Walbot (2011). Cell types are color coded: orange is epidermis (EP); green is endothecium (EN); red is middle layer (ML); blue is tapetum (TAP); pink is meiocyte (M); white is vascular/connective.

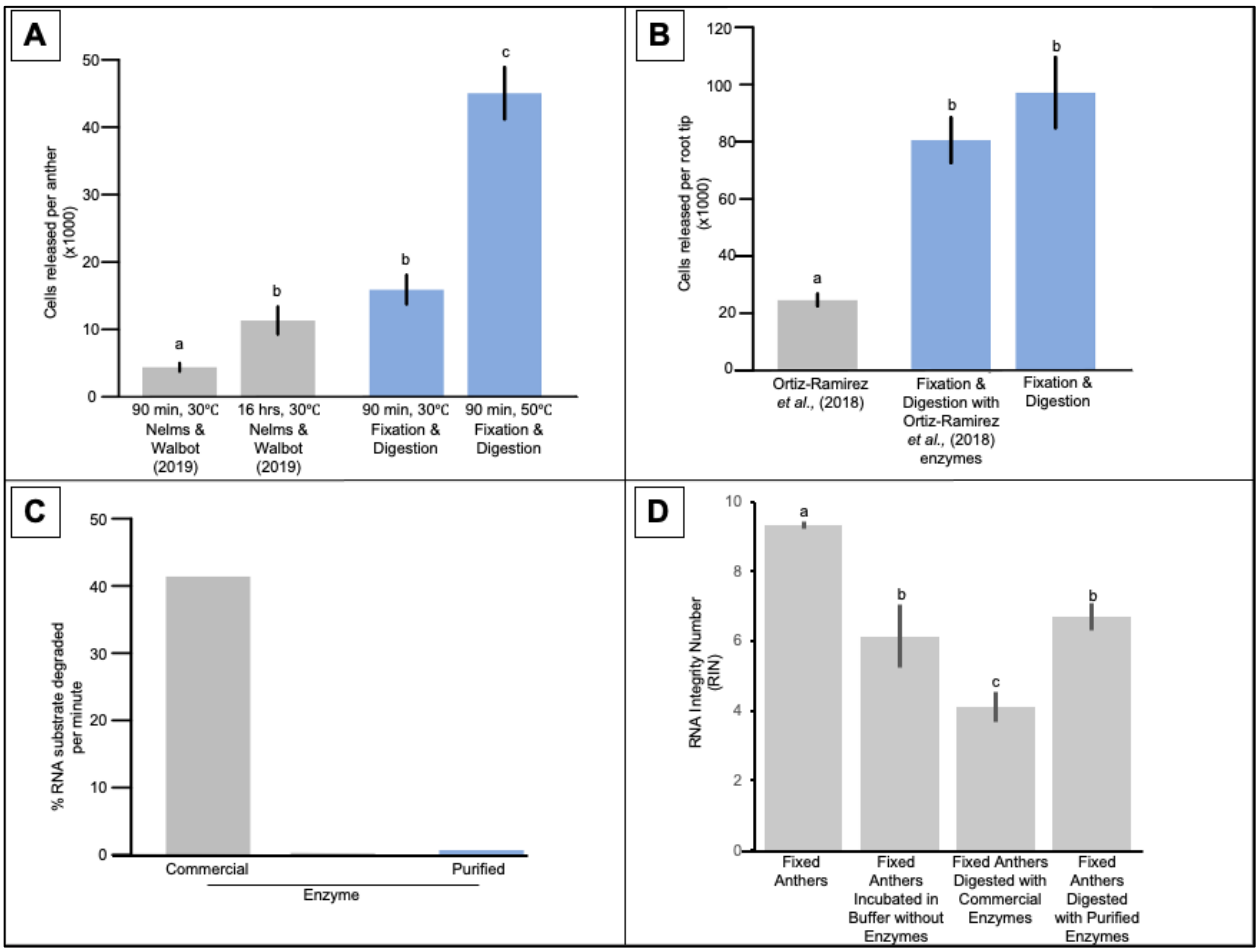

Figure 2. Cellular release and RNA integrity of fresh and fixed protoplasting protocols. (A) Maize anthers were digested for 90 min or 16 h at 30°C following the Nelms and Walbot (2019) protoplasting protocol, and cell release quantified via hemocytometer (grey bars). Fixed maize anthers were digested for 90 min at 30°C and 50°C using the reduced enzyme mix and cell release similarly quantified (blue bars). (B) Cellular release of maize root tips comparing the optimized protoplasting protocol from Ortiz-Ramirez *et al.* (2018) and the fixation-based protocol. Maize root tips were digested following Ortiz-Ramírez *et al.* (2018) and cell release quantified via hemocytometer (grey bars). Maize root tips were fixed then digested at 50°C for 90 min using the Ortiz-Ramírez *et al.* (2018) protoplast enzyme mix and the reduced enzyme mix then cell release was similarly quantified (blue bars). (C) RNA degradation rate of commercial versus purified enzyme mix. (D) RNA quality of fixed maize anthers without any digestion, fixed maize anthers that were digested at 50°C for 90 min in enzyme buffer lacking enzymes, fixed maize anther that were digested at 50°C for 90 min using commercial enzyme

mix, and fixed maize anthers that were digested at 50°C for 90 min using purified enzyme mix. Different letters denote statistically significant variation (Student's *t* test, $P < 0.05$) and error bars represent standard error.

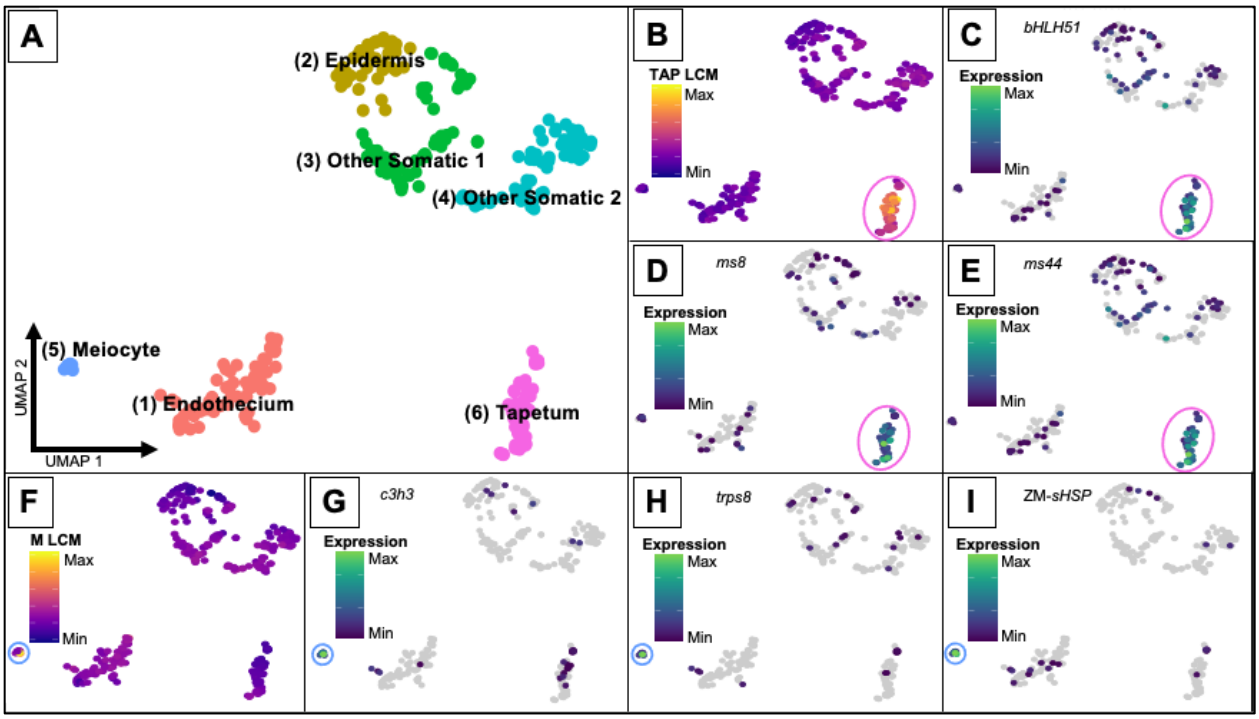

Figure 3. Maize anther scRNA-seq of tapetum and meiocyte marker genes. (A) UMAP clustering of 307 cells from 2.0 mm maize anthers into six distinct clusters. (B) Correlation values of each cell with LCM tapetal data. (C-E) Expression values per maize anther cell of tapetal marker genes mapped onto the UMAP clusters. (F) Correlation values of each cell with LCM meiocyte data. (G-I) Expression values per maize anther cell of meiocyte marker genes mapped onto the UMAP clusters.

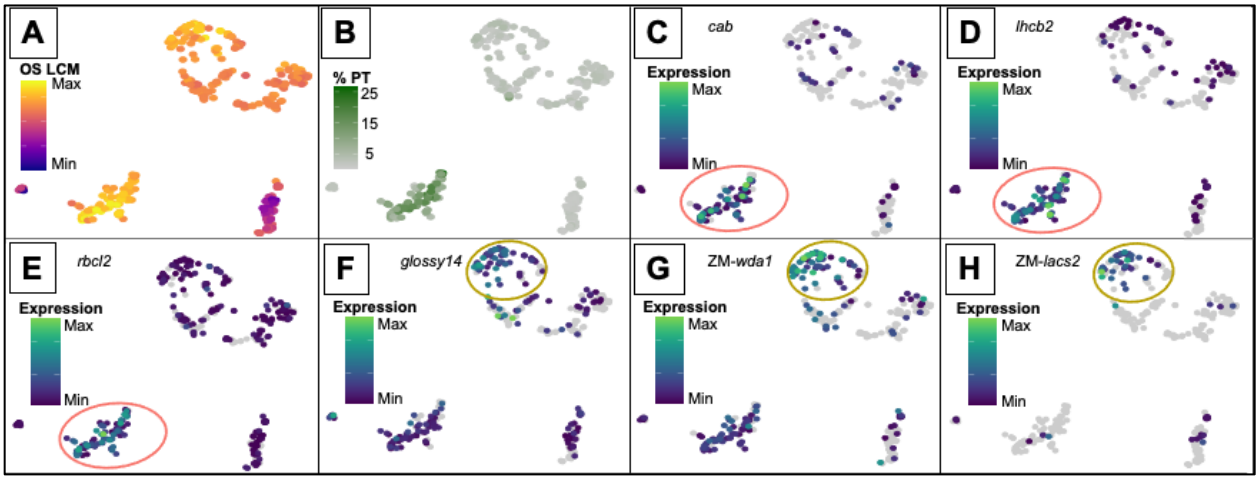

Figure 4. Endothecium and epidermis marker gene expression in maize anther cells. (A) Correlation values of each cell with LCM other somatic cell types (middle layer, endothecium, epidermis) data. (B) Percentage of total UMIs originating from the plastid for each cell. (C-E) Expression values per maize anther cell of putative endothecium marker genes mapped onto the UMAP clusters. (F-H) Expression values per maize anther cell of putative epidermis marker genes mapped onto the UMAP clusters.

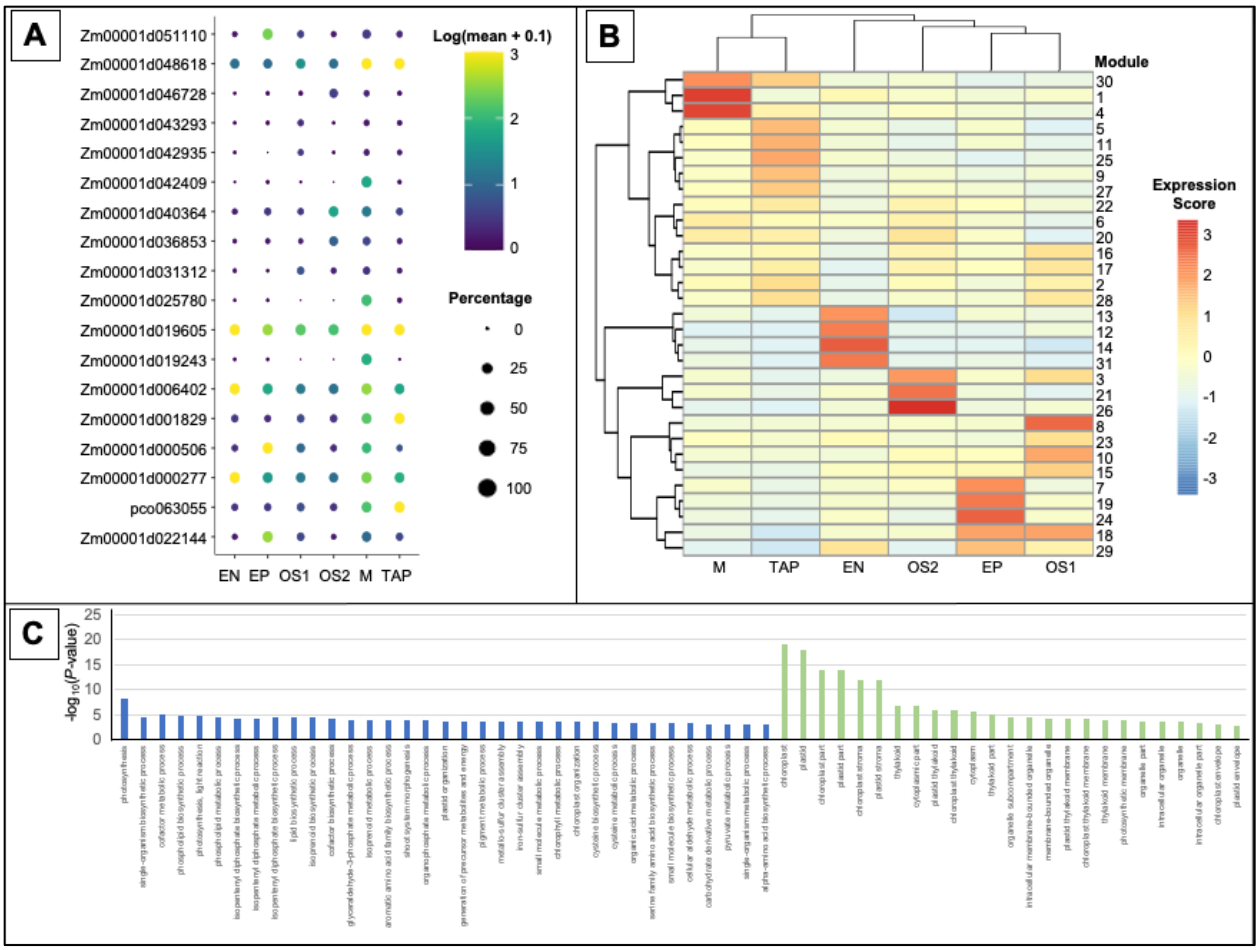

Figure 5. *De novo* marker gene identification and co-regulated gene modules. (A) Top three marker genes for each UMAP cluster with expression and percentage of cells from each cluster expressing the gene. (B) Co-regulated gene modules and expression scores for each UMAP cluster. (C) Gene ontology (GO) enrichment analysis of Module 31 sorted by biological processes (blue bars) and cellular component (green bars). Significantly enriched GO terms were selected based on a false discovery rate (FDR) < 0.05.

Parsed Citations

Aronesty, E. (2013). Comparison of sequencing utility programs, Open Bioinf. J 7: 1–8.
Google Scholar: Author Only Title Only Author and Title

Cao, J., Spielmann, M., Qiu, X., Huang, X., Ibrahim, D.M., Hill, A.J., Zhang, F., Mundlos, S., Christiansen, L., and Steemers, F.J. (2019). The single-cell transcriptional landscape of mammalian organogenesis. Nature 566: 496–502.
Google Scholar: Author Only Title Only Author and Title

Chaubal, R., Zanella, C., Trimnell, M.R., Fox, T.W., Albertsen, M.C., and Bedinger, P. (2000). Two male-sterile mutants of Zea mays (Poaceae) with an extra cell division in the anther wall. Am. J. Bot. 87: 1193–1201.
Google Scholar: Author Only Title Only Author and Title

Chen, S., Zhou, Y., Chen, Y., and Gu, J. (2018). fastp: an ultra-fast all-in-one FASTQ preprocessor. Bioinformatics 34: i884–i890.
Google Scholar: Author Only Title Only Author and Title

Conde, D., Triozzi, P.M., Balmant, K.M., Doty, A.L., Miranda, M., Boullosa, A., Schmidt, H.W., Pereira, W.J., Dervinis, C., and Kirst, M. (2021). A robust method of nuclei isolation for single-cell RNA sequencing of solid tissues from the plant genus Populus. PLoS One 16: e0251149.
Google Scholar: Author Only Title Only Author and Title

Denyer, T., Ma, X., Klesen, S., Scacchi, E., Nieselt, K., and Timmermans, M.C.P. (2019). Spatiotemporal developmental trajectories in the Arabidopsis root revealed using high-throughput single-cell RNA sequencing. Dev. Cell 48: 840-852.e5.
Google Scholar: Author Only Title Only Author and Title

Fields, R., Dixon, H.B., Law, G.R., and Yui, C. (1971). Purification of ribonuclease T 1 by diethylaminoethylcellulose chromatography. Biochem. J. 121: 591–596.
Google Scholar: Author Only Title Only Author and Title

Fox, T., DeBruin, J., Haug Collet, K., Trimnell, M., Clapp, J., Leonard, A., Li, B., Scolaro, E., Collinson, S., and Glassman, K. (2017). A single point mutation in Ms44 results in dominant male sterility and improves nitrogen use efficiency in maize. Plant Biotechnol. J. 15: 942–952.
Google Scholar: Author Only Title Only Author and Title

Han, X. et al. (2020). Construction of a human cell landscape at single-cell level. Nature 581: 303–309.
Google Scholar: Author Only Title Only Author and Title

Hashimshony, T., Senderovich, N., Avital, G., Klochendler, A., de Leeuw, Y., Anavy, L., Gennert, D., Li, S., Livak, K.J., and Rozenblatt-Rosen, O. (2016). CEL-Seq2: sensitive highly-multiplexed single-cell RNA-Seq. Genome Biol. 17: 77.
Google Scholar: Author Only Title Only Author and Title

Jean-Baptiste, K., McFaline-Figueroa, J.L., Alexandre, C.M., Dorrity, M.W., Saunders, L., Bubb, K.L., Trapnell, C., Fields, S., Queitsch, C., and Cuperusa, J.T. (2019). Dynamics of gene expression in single root cells of Arabidopsis thaliana. Plant Cell 31: 993–1011.
Google Scholar: Author Only Title Only Author and Title

Jiao, Y. et al. (2017). Improved maize reference genome with single-molecule technologies. Nature 546: 524–527.
Google Scholar: Author Only Title Only Author and Title

Jung, K.-H., Han, M.-J., Lee, D., Lee, Y.-S., Schreiber, L., Franke, R., Faust, A., Yephremov, A., Saedler, H., Kim, Y.-W., Hwang, I., and An, G. (2006). Wax-deficient anther1 is involved in cuticle and wax production in rice anther walls and is required for pollen development. Plant Cell 18: 3015–3032.
Google Scholar: Author Only Title Only Author and Title

Kanaya, S. and Uchida, T. (1981). Purification of ribonuclease T1 by affinity chromatography. J. Biochem. 89: 591–597.
Google Scholar: Author Only Title Only Author and Title

Kanton, S. et al. (2019). Organoid single-cell genomic atlas uncovers human-specific features of brain development. Nature 574: 418–422.
Google Scholar: Author Only Title Only Author and Title

Kelliher, T. and Walbot, V. (2011). Emergence and patterning of the five cell types of the Zea mays anther locule. Dev. Biol. 350: 32–49.
Google Scholar: Author Only Title Only Author and Title

Kim, D., Paggi, J.M., Park, C., Bennett, C., and Salzberg, S.L. (2019). Graph-based genome alignment and genotyping with HISAT2 and HISAT-genotype. Nat. Biotechnol. 37: 907–915.
Google Scholar: Author Only Title Only Author and Title

Li, H., Handsaker, B., Wysoker, A., Fennell, T., Ruan, J., Homer, N., Marth, G., Abecasis, G., and Durbin, R. (2009). The sequence alignment/map format and SAMtools. Bioinformatics 25: 2078–2079.
Google Scholar: Author Only Title Only Author and Title

Lim, B., Lin, Y., and Navin, N. (2020). Advancing Cancer Research and Medicine with Single-Cell Genomics. Cancer Cell 37: 456–470.
Google Scholar: Author Only Title Only Author and Title

Liu, Q., Liang, Z., Feng, D., Jiang, S., Wang, Y., Du, Z., Li, R., Hu, G., Zhang, P., Ma, Y., Lohmann, J.U., and Gu, X. (2021). Transcriptional landscape of rice roots at the single-cell resolution. Mol. Plant 14: 384–394.
Google Scholar: Author Only Title Only Author and Title

Lopez-Anido, C.B., Vatén, A., Smoot, N.K., Sharma, N., Guo, V., Gong, Y., Anleu Gil, M.X., Weimer, A.K., and Bergmann, D.C. (2021). Single-cell resolution of lineage trajectories in the Arabidopsis stomatal lineage and developing leaf. Dev. Cell 56: 1043-1055.e4.
Google Scholar: Author Only Title Only Author and Title

MacIntosh, G.C. (2011). RNase T2 Family: enzymatic properties, functional diversity, and evolution of ancient ribonucleases BT - Ribonucleases. In A.W. Nicholson, ed (Springer Berlin Heidelberg: Berlin, Heidelberg), pp. 89–114.
Google Scholar: Author Only Title Only Author and Title

McInnes, L., Healy, J., and Melville, J. (2020). UMAP: uniform manifold approximation and projection for dimension reduction.

Mi, H., Ebert, D., Muruganujan, A., Mills, C., Albou, L.-P., Mushayamaha, T., and Thomas, P.D. (2021). PANTHER version 16: a revised family classification, tree-based classification tool, enhancer regions and extensive API. Nucleic Acids Res. 49: D394–D403.
Google Scholar: Author Only Title Only Author and Title

Nan, G., Zhai, J., Arikit, S., Morrow, D., Fernandes, J., Mai, L., Nguyen, N., Meyers, B.C., and Walbot, V. (2017). MS23 , a master basic helix-loop-helix factor , regulates the specification and development of the tapetum in maize.: 163–172.
Google Scholar: Author Only Title Only Author and Title

Nelms, B. and Walbot, V. (2019). Defining the developmental program leading to meiosis in maize. Science (80-.). 364: 52–56.
Google Scholar: Author Only Title Only Author and Title

Ortiz-Ramírez, C., Arevalo, E.D., Xu, X., Jackson, D.P., and Birnbaum, K.D. (2018). An efficient cell sorting protocol for maize protoplasts. Curr. Protoc. plant Biol. 3: e20072.
Google Scholar: Author Only Title Only Author and Title

Paik, D.T., Cho, S., Tian, L., Chang, H.Y., and Wu, J.C. (2020). Single-cell RNA sequencing in cardiovascular development, disease and medicine. Nat. Rev. Cardiol. 17: 457–473.
Google Scholar: Author Only Title Only Author and Title

Pardo, A.G. and Forchiassin, F. (1999). Influence of temperature and pH on cellulase activity and stability in Nectria catalinensis. Rev. Argent. Microbiol. 31: 31–35.
Google Scholar: Author Only Title Only Author and Title

R Core Team (2013). R: A language and environment for statistical computing.

Rosenberg, A.B. et al. (2018). Single-cell profiling of the developing mouse brain and spinal cord with split-pool barcoding. Science (80-.). 360: 176–182.
Google Scholar: Author Only Title Only Author and Title

Ryu, K.H., Huang, L., Kang, H.M., and Schiefelbein, J. (2019). Single-cell RNA sequencing resolves molecular relationships among individual plant cells. Plant Physiol. 179: 1444–1456.
Google Scholar: Author Only Title Only Author and Title

Schnurr, J., Shockey, J., and Browse, J. (2004). The acyl-CoA synthetase encoded by LACS2 is essential for normal cuticle development in Arabidopsis. Plant Cell 16: 629–642.
Google Scholar: Author Only Title Only Author and Title

Seyfferth, C., Renema, J., Wendrich, J.R., Eekhout, T., Seurinck, R., Vandamme, N., Blob, B., Saeys, Y., Helariutta, Y., Birnbaum, K.D., and De Rybel, B. (2021). Advances and opportunities in single-cell transcriptomics for plant research. Annu. Rev. Plant Biol. 72: 847–866.
Google Scholar: Author Only Title Only Author and Title

Smith, T., Heger, A., and Sudbery, I. (2017). UMI-tools: modeling sequencing errors in Unique Molecular Identifiers to improve quantification accuracy. Genome Res. 27: 491–499.
Google Scholar: Author Only Title Only Author and Title

Sunaga-Franze, D.Y., Muino, J.M., Braeuning, C., Xu, X., Zong, M., Smaczniak, C., Yan, W., Fischer, C., Vidal, R., Kliem, M., Kaufmann, K., and Sauer, S. (2021). Single-nuclei RNA-sequencing of plant tissues. bioRxiv: 2020.11.14.382812.
Google Scholar: Author Only Title Only Author and Title

Team, Rs. (2015). RStudio: integrated development for R. RStudio, Inc., Boston, MA URL http//www. rstudio. com 42: 84.
Google Scholar: Author Only Title Only Author and Title

Thrupp, N., Frigerio, C.S., Wolfs, L., Skene, N.G., Fattorelli, N., Poovathingal, S., Fourne, Y., Matthews, P.M., Theys, T., and Mancuso, R. (2020). Single-nucleus RNA-Seq is not suitable for detection of microglial activation genes in humans. Cell Rep. 32: 108189.
Google Scholar: Author Only Title Only Author and Title

Tian, T., Liu, Y., Yan, H., You, Q., Yi, X., Du, Z., Xu, W., and Su, Z. (2017). agriGO v2. 0: a GO analysis toolkit for the agricultural community, 2017 update. Nucleic Acids Res. 45: W122–W129.

Google Scholar: Author Only Title Only Author and Title

Walbot, V. and Egger, R.L. (2016). Pre-meiotic anther development: cell fate specification and differentiation. Annu. Rev. Plant Biol. 67: 365–395.
Google Scholar: Author Only Title Only Author and Title

Wang, D., Oses-Prieto, J.A., Li, K.H., Fernandes, J.F., Burlingame, A.L., and Walbot, V. (2010). The male sterile 8 mutation of maize disrupts the temporal progression of the transcriptome and results in the mis-regulation of metabolic functions. Plant J. 63: 939–951.
Google Scholar: Author Only Title Only Author and Title

Zhang, T.Q., Xu, Z.G., Shang, G.D., and Wang, J.W. (2019). A single-cell RNA sequencing profiles the developmental landscape of Arabidopsis root. Mol. Plant 12: 648–660.
Google Scholar: Author Only Title Only Author and Title

Zheng, J., He, C., Qin, Y., Lin, G., Park, W.D., Sun, M., Li, J., Lu, X., Zhang, C., and Yeh, C. (2019). Co-expression analysis aids in the identification of genes in the cuticular wax pathway in maize. Plant J. 97: 530–542.
Google Scholar: Author Only Title Only Author and Title

Zhou, X., Huang, K., Teng, C., Batish, M., Meyers, B.C., and Walbot, V. (2021). 24-nt phasiRNAs move from tapetal to meiotic cells in maize anthers. bioRxiv: 2021.08.24.457464.
Google Scholar: Author Only Title Only Author and Title